Electronic Supplementary Material (ESI) for Journal of Materials Chemistry A.

Supporting Information

p-n fusion strategy to design bipolar organic materials for high-energy-density symmetric batteries

Jihyeon Kim[1†], Heechan Kim[2†], Sechan Lee[1], Giyun Kwon[1], Taewon Kang[2], Hyeokjun Park[1], Orapa Tamwattana[1], Youngmin Ko[1], Dongwhan Lee[2], and Kisuk Kang[1,3,4,5]**

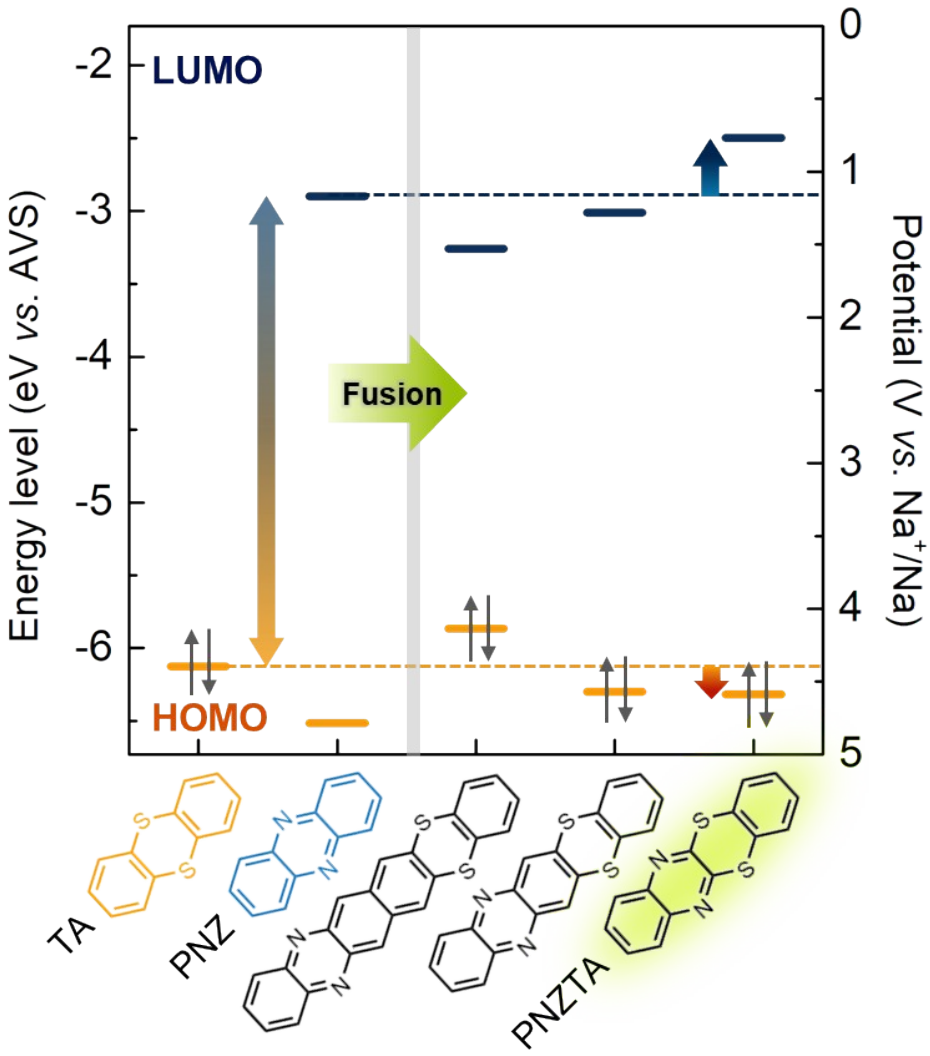

Figure S1. Calculated HOMO and LUMO level of TA, PNZ and various fused molecules of those motifs. The Na/Na^+ redox potential was set to −1.73 V versus AVS because the standard hydrogen electrode (SHE) is −4.44 V versus AVS and Na/Na^+ is −2.71 V versus SHE.

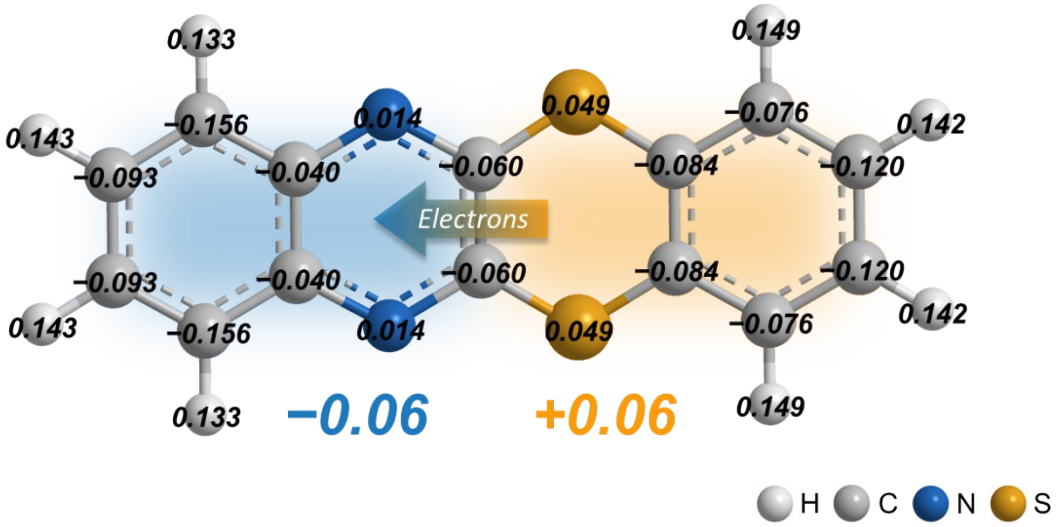

Figure S2. Charge distribution calculation of PNZTA using natural population analysis.

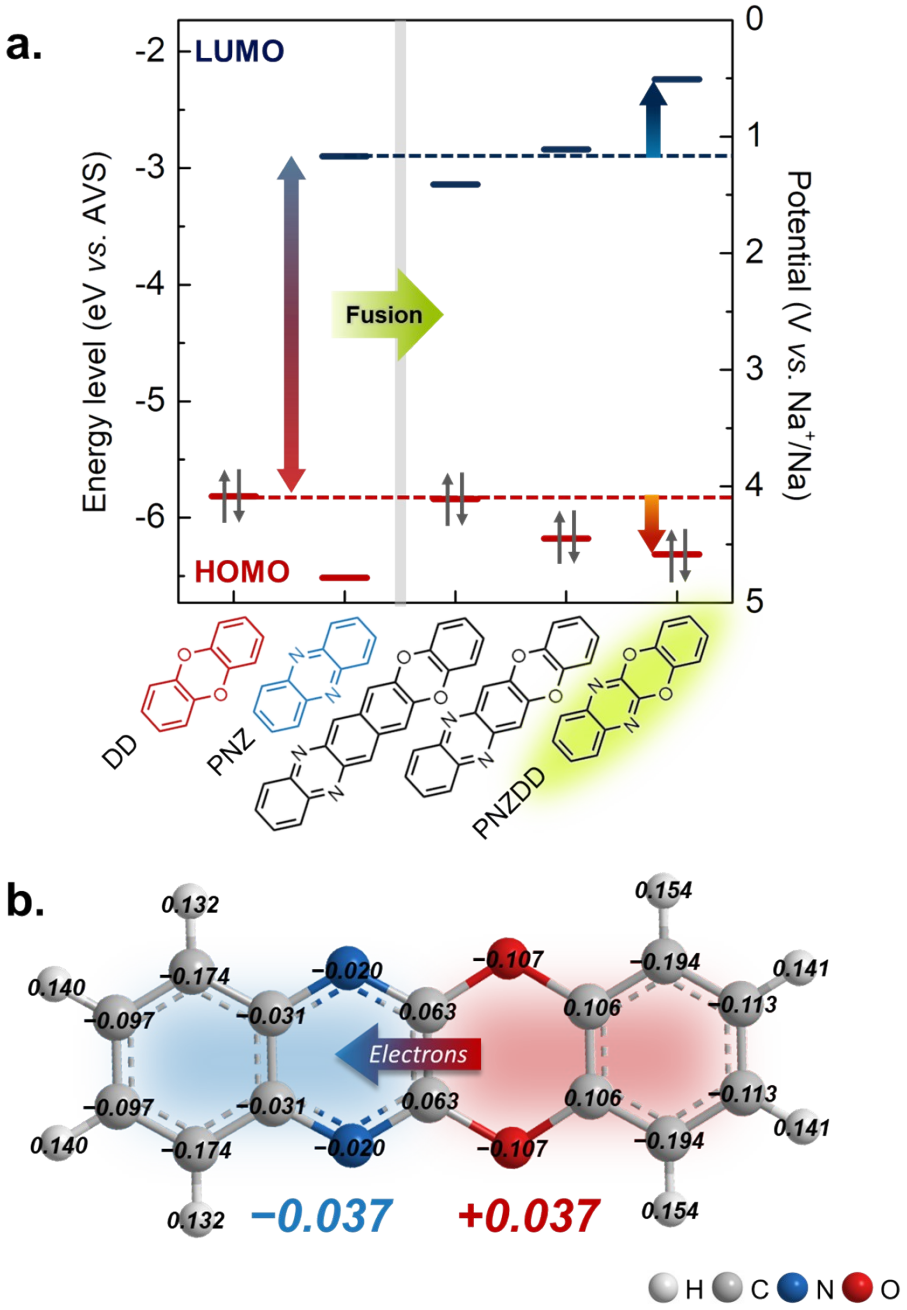

Figure S3. The *p–n* fusion of DD and PNZ. a) Calculated molecular orbital energies (HOMO and LUMO) of DD, PNZ and various fused molecules of those motifs. The Na/Na^+ redox potential was set to −1.73 V versus AVS because the SHE is −4.44 V versus AVS and Na/Na^+ is −2.71 V versus SHE. b) Charge distribution calculation of PNZDD using natural population analysis.

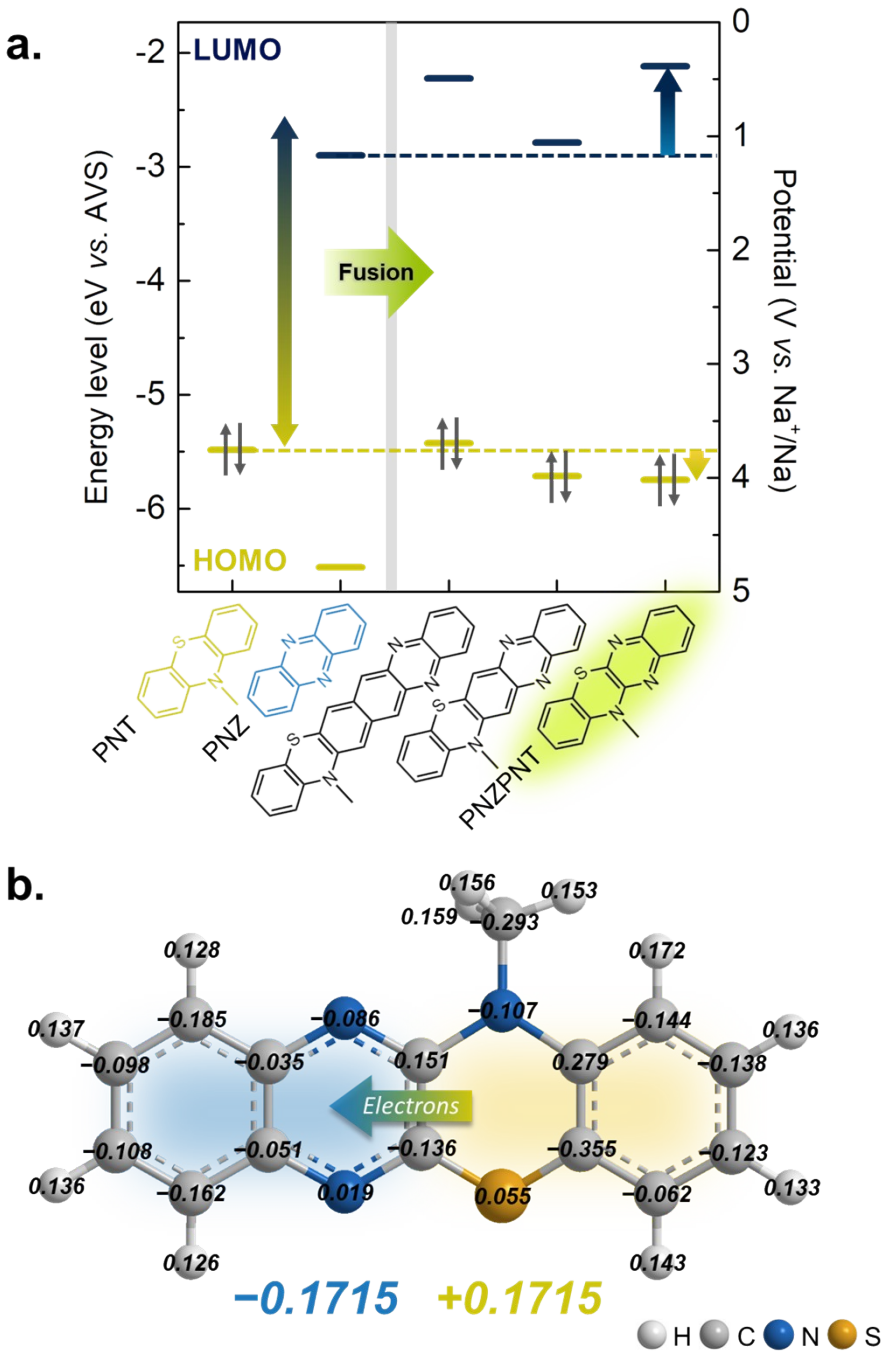

Figure S4. The *p–n* fusion of PTZ and PNZ. a) Calculated molecular orbital energies (HOMO and LUMO) of PTZ, PNZ and various fused molecules of those motifs. b) Charge distribution calculation of PNZPTZ using natural population analysis.

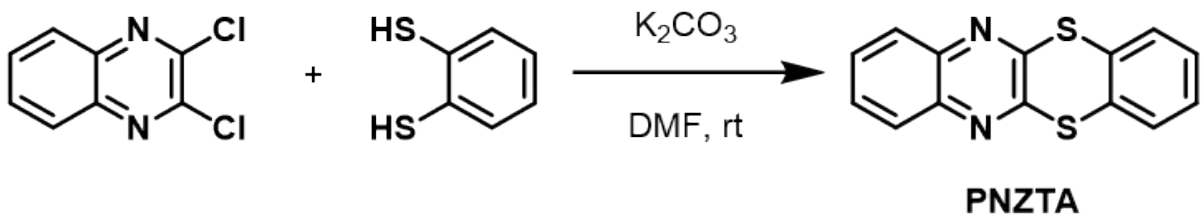

Figure S5. Synthetic scheme for PNZTA.

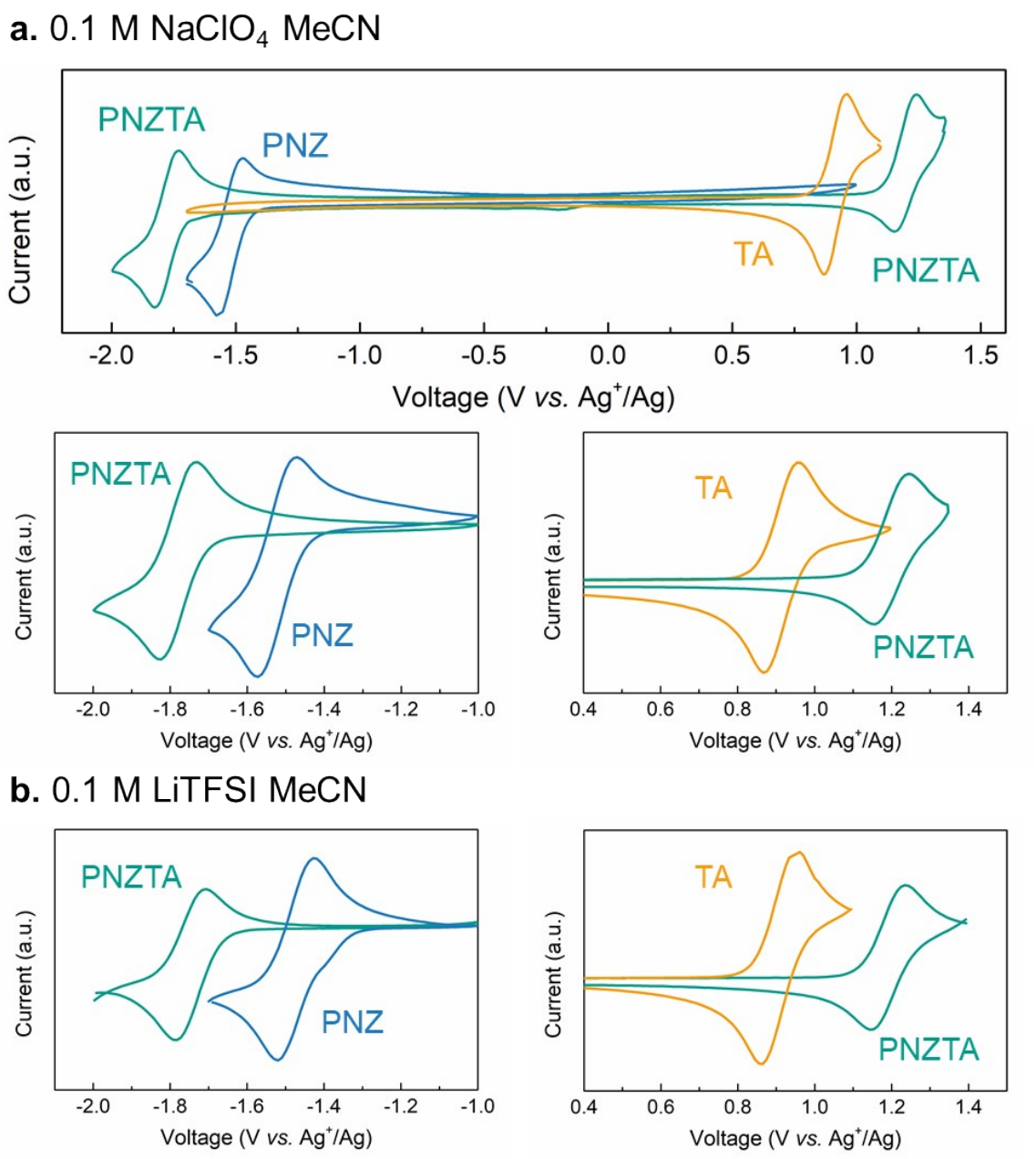

Figure S6. CV results of PNZ, TA and PNZTA in various electrolyte system. a) 0.1 M $NaClO_4$ in MeCN, b) 0.1 M LiTFSI in MeCN

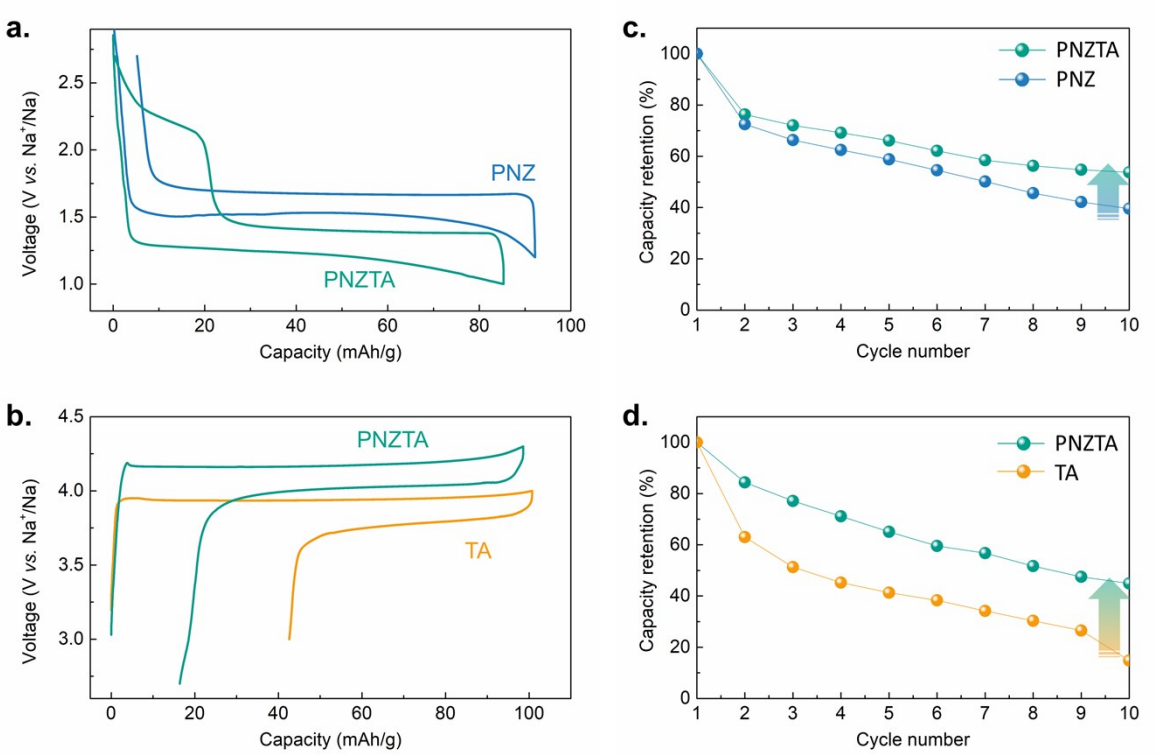

Figure S7. Galvanostatic charge/discharge profile and capacity retention curves of PNZ, TA, and PNZTA half-cell at a current density of C/5. a, c) The *n*-type redox reaction of PNZ and PNZTA. b,d) The *p*-type redox reaction of TA and PNZTA.

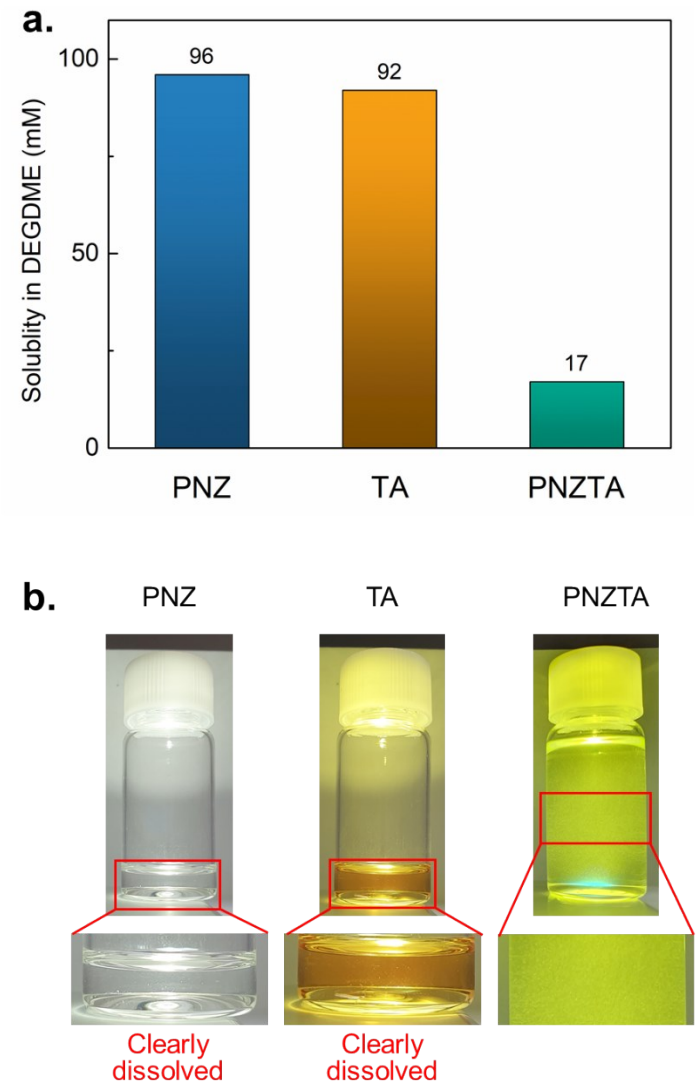

Figure S8. Solubility test for PNZ, TA and PNZTA. a) Powder solubility of PNZ, TA and PNZTA in DEGDEM solvent which was used in this paper b) Images of solvent after dissolving each material. PNZTA showed significantly low solubility than PNZ and TA.

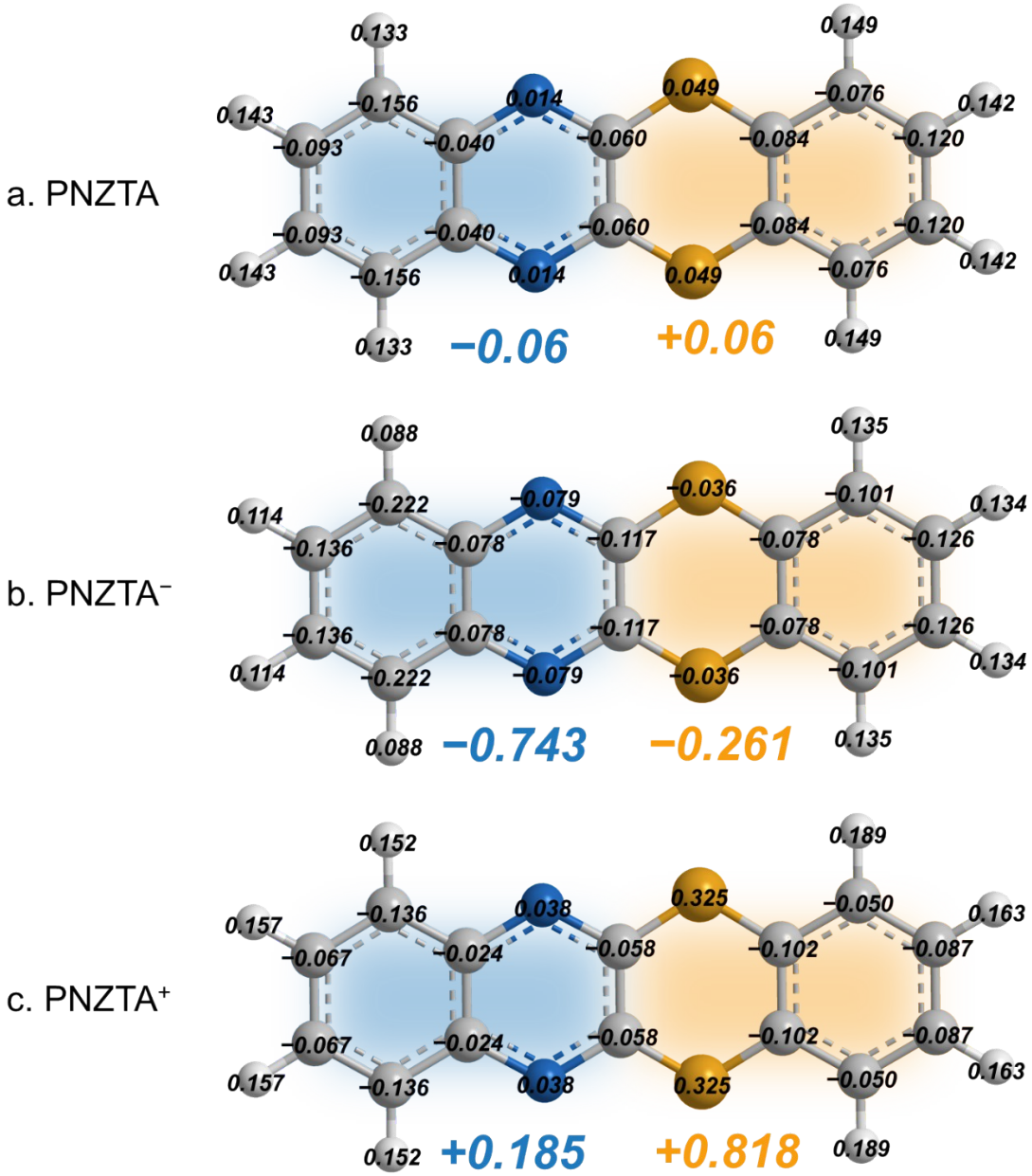

Figure S9. Charge distribution calculations of a) PNZTA, b) PNZTA^{-}, and c) PNZTA^{+} using natural population analysis. The numbers on each atom denotes the calculated atomic charges. The numbers under each molecule are the sum of atomic charges which corresponding to the phenazine motif (blue) and the thianthrene motif (orange), respectively.

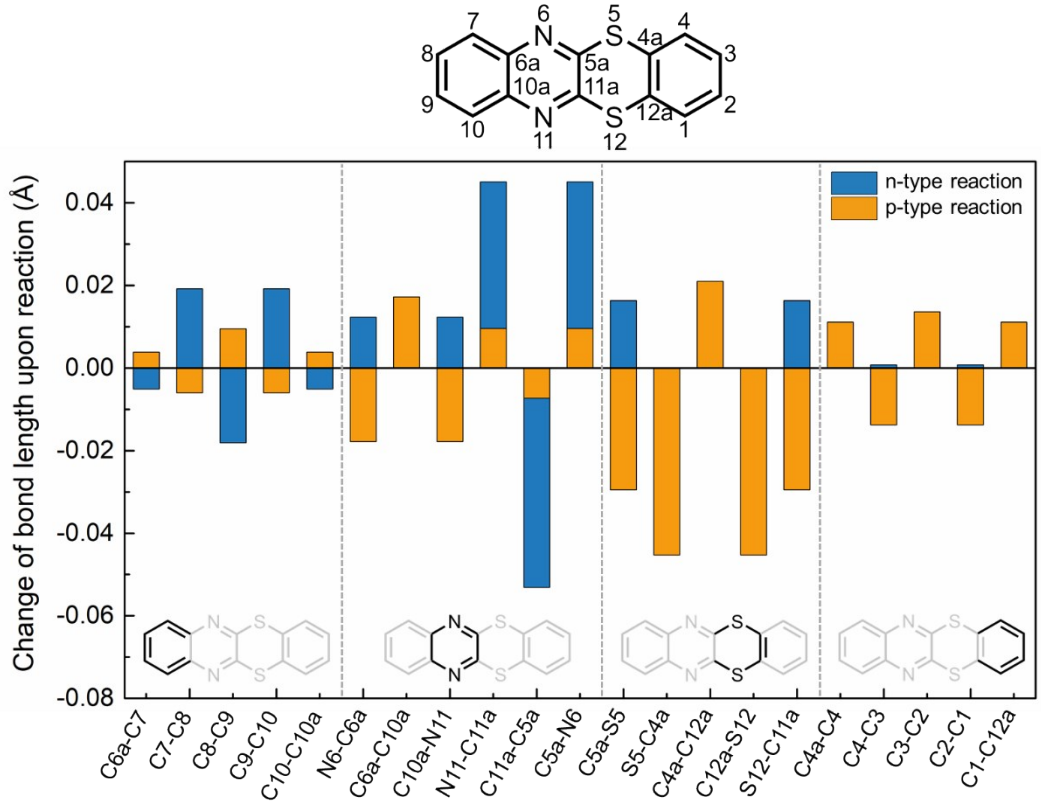

Figure S10. The bond length changes of PNZTA upon reduction (that is n-type reaction, blue bar) and oxidation (that is p-type reaction, orange bar)

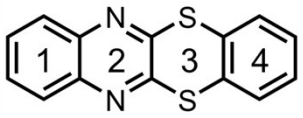

Wavenumber (cm^{-1})	Vibrational mode
433	Wagging of C-C-C, C-N=C, C-S-C, and C-C-C bonds in ring 1,2,3, and 4 respectively
612	In-plane scissoring of C-C-C bonds in ring 1
1125	In-plane symmetical stretching of C-C-C bonds in between ring 3 and 4 In-plane asymmetrical stretching of C-C-S bonds in ring 3
1137	In-plane symmetrical stretching of C-C-C bonds in between ring 1 and ring 2 In-plane asymmetrical stretching of C-C-N bonds in ring 2
1152	In-plane scissoring of C-C-C bonds in ring 1 In-plane scissoring of C-N=C bonds in ring 2
1199	In-plane scissoring of C-C-H bonds in ring 1
1285	In-plane asymmetrical stretching of C-C=C bonds in ring 1 In-plane asymmetrical stretching of C-N=C bonds in ring 2
1392	In-plane assymmetrical stretching of C-C=C bonds bonds in ring 1 In-plane assymmetrical stretching of C-C=N bonds in between ring 1 and 2

Figure S11. Peak assignments for FT-IR spectra.

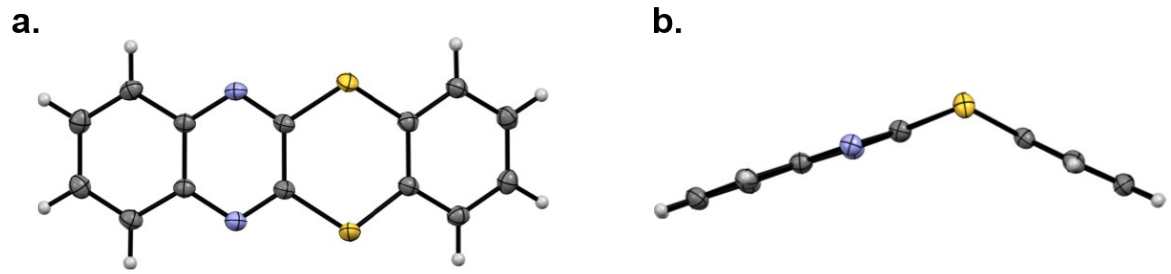

Figure S12. X-ray structure of PNZTA: a) top view and b) side view.

	PNZTA
Chemical formula	$C_{14}H_8N_2S_2$
Formula weight	268.34
Crystal system	triclinic
Space group	P-1
Color of crystal	fluorescence yellow
a (Å)	6.9896(3)
b (Å)	9.2152(4)
c (Å)	9.6542(3)
α (°)	100.010(3)
β (°)	94.635(3)
γ (°)	105.365(3)
Volume (Å^3)	585.19(4)
Z	2
R(int)	0.0281
Final R indices [I > 2σ(I)]	R_1 = 0.0408, wR_2 = 0.1205
Final R indices [all data]	R_1 = 0.0418, wR_2 = 0.1216
GOF	1.090

Table S1. Summary of X-ray crystallographic data.

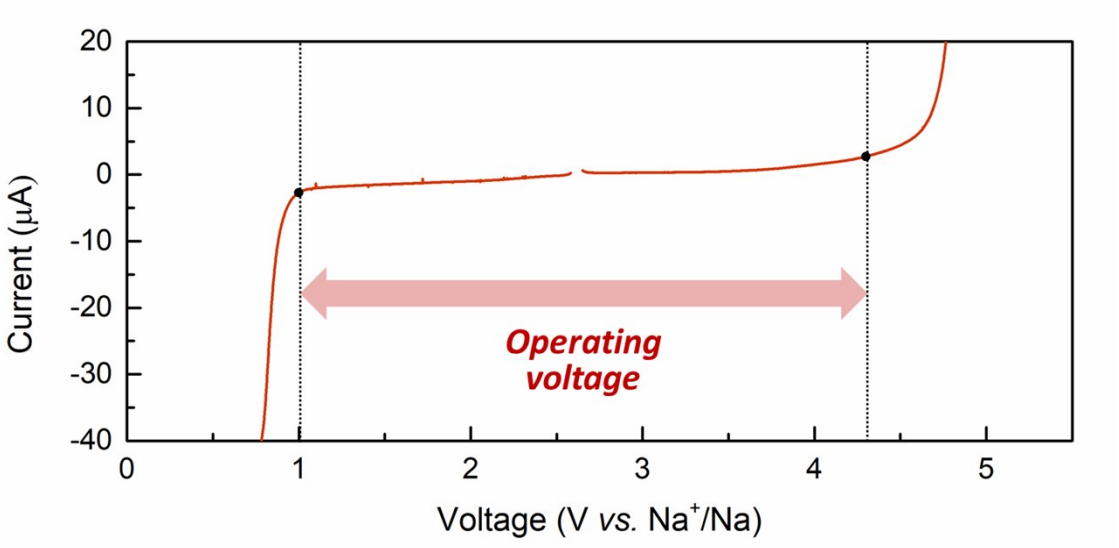

Figure S13. Linear sweep voltammetry (LSV) curves of Na metal / 3.5 m $NaClO_4$ in DEGDME / SUS cell.

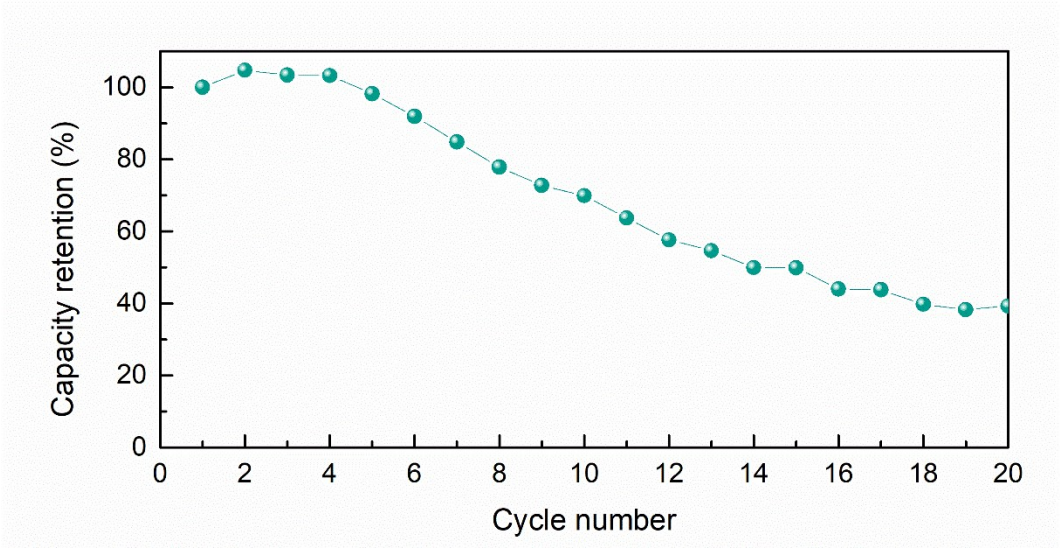

Figure S14. Capacity retentions of PNZTA symmetric cell after the activation cycle.

Compounds	Average Voltage (V)	Capacity (mAh/g, based on the weight of one electrode)	Reference
$Li_7V_{15}O_{36}(CO_3)$	1.2	120	1
$Na_3MnTi(PO_4)_3$	1.3	57.9	2
$Li_{1.5}Cr_{0.5}Ti_{1.5}(PO_4)_3$	2.15	32	3
$Na_3V_2(PO_4)_3$	1.8	90.2	4
$Na_2LiV_2(PO_4)_3/C$	1.08	95	5
$Na_{0.8}Ni_{0.4}Ti_{0.6}O_2$	2.8	85	6
$Na_{0.6}Cr_{0.6}Ti_{0.4}O_2$	2.53	74	7
$N_a2VTi(PO_4)_3$	1.2	72	8
$Na_3Co_{0.5}Mn_{0.5}Ti(PO_4)_3$	1.4	43	9
$Na_3V_2(PO_4)_2F_3/C$	2.53	107	10
$Li_3V_{2(}PO_4)_3/C$	1.85	87	11
$Na_4C_8H_2O_6$	1.8	198	12
$K_3C_6O_6$	1.1	70	13
$Na_4C_6O_6$	0.65	167	14
$Li_4C_8H_2O_6$	1.8	208	15
$C_{52}H_{62}N_4O_{23}Li_4$	2.5	53	16
$Li_4C_6O_6$	0.65	178	17

Table S2. Performance of previous reported symmetric cells. The energy densities of the symmetric cells were estimated with respect to the weight of one electrode.

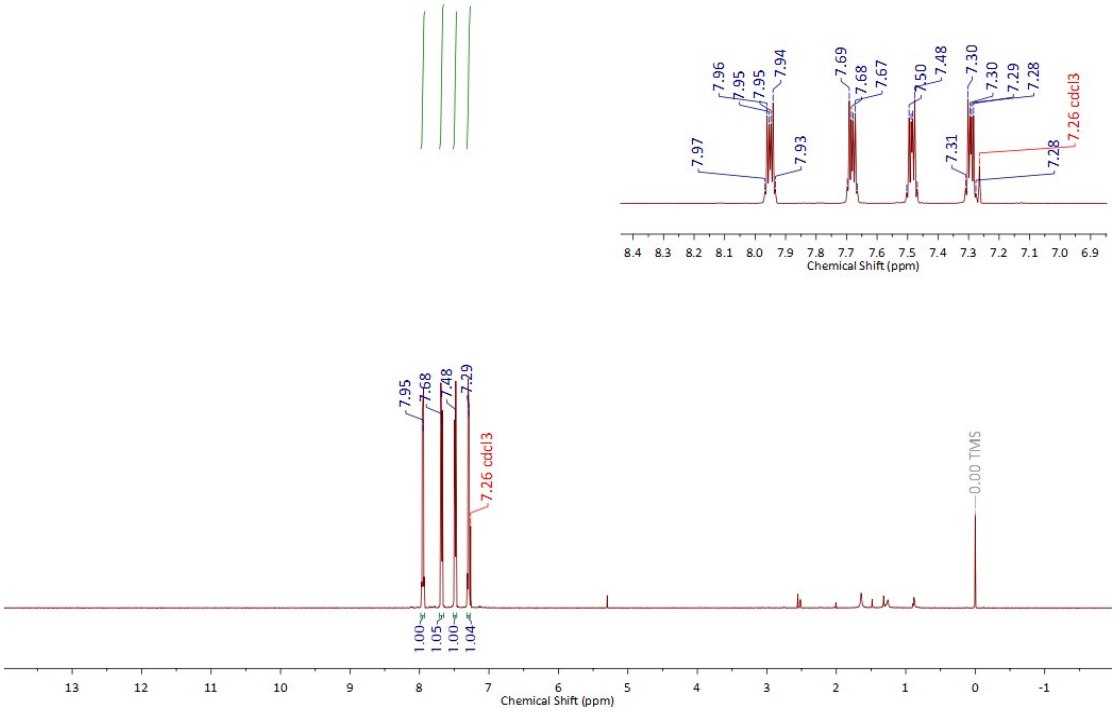

Figure S15. ^{1}H NMR (500 MHz) spectrum of **PNZTA** in $CDCl_3$ (T = 298 K)

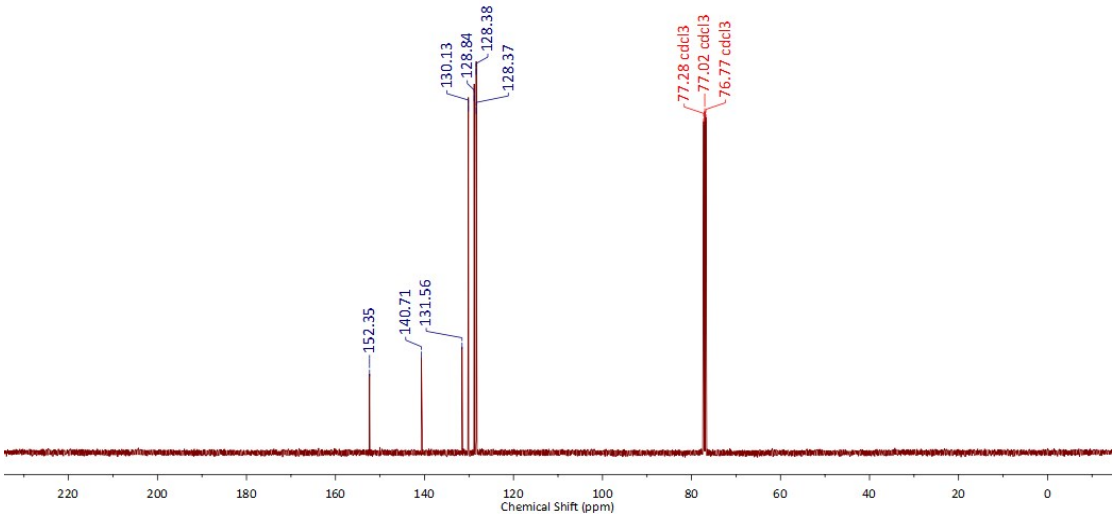

Figure S16. ^{13}C NMR (125 MHz) spectrum of **PNZTA** in $CDCl_3$ (T = 298 K)

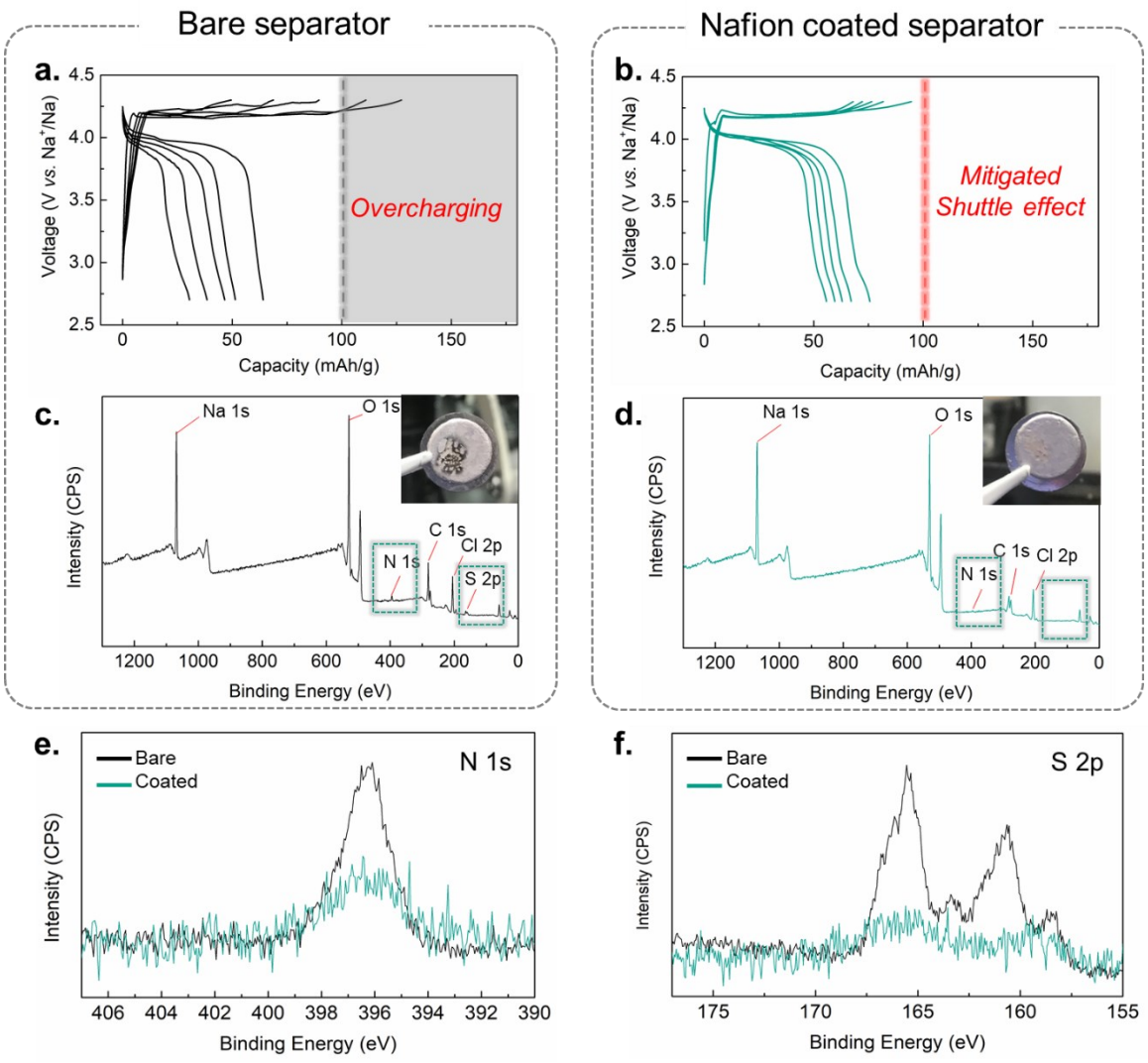

Figure S17. Preventing shuttle effect of PNZTA through separator engineering. a, b) Charge/discharge curves of p-type reaction of PNZTA utilizing celgard separator(a) and nafion coated separator (b). Overcharging due to the shuttle effect was mitigated after using nafion coated separator. c, d) XPS survey scan results and surface images for Na metal anode after charging the PNZTA half cells using celgard separator(c) and nafion coated separator (d). e, f) Comparison of XPS narrow scan results of N 1s (e) and S 2p (f) spectra from the results of c) and d). In the cell using only celgard separator, the nitrogen and sulfur which is originated from PNZTA was found in the metal surface resulting in the contamination of metal surface. However, after using nafion coated separator, sodium metal retained a clean pristine surface

after charging and none of nitrogen and sulfur was found in the surface, indicating the suppression of PNZTA migration from cathode to anode.

References

1. Chen, J.-J., Ye, J.-C., Zhang, X.-G., Symes, M.D., Fan, S.-C., Long, D.-L., Zheng, M.-S., Wu, D.-Y., Cronin, L., and Dong, Q.-F. (2018). Design and Performance of Rechargeable Sodium Ion Batteries, and Symmetrical Li-Ion Batteries with Supercapacitor-Like Power Density Based upon Polyoxovanadates. *Adv. Energy Mater.* ***8***, 1701021.

2. Gao, H., and Goodenough, J.B. (2016). An Aqueous Symmetric Sodium-Ion Battery with NASICON-Structured $Na_3MnTi(PO_4)_3$. *Angew. Chem. Int. Ed.* ***55***, 12768-12772.

3. Inoishi, A., Nishio, A., Yoshioka, Y., Kitajou, A., and Okada, S. (2018). A single-phase all-solid-state lithium battery based on $Li_{1.5}Cr_{0.5}Ti_{1.5}(PO_4)_3$ for high rate capability and low temperature operation. *ChemComm* ***54***, 3178-3181.

4. Zhang, Y., Zhao, H., and Du, Y. (2016). Symmetric full cells assembled by using self-supporting $Na_3V_2(PO_4)_3$ bipolar electrodes for superior sodium energy storage. *J. Mater. Chem. A* ***4***, 7155-7159.

5. Li, M., Zuo, Z., Deng, J., Yao, Q., Wang, Z., Zhou, H., Luo, W.-B., Liu, H.-K., and Dou, S.-X. (2018). A high rate capability and long lifespan symmetric sodium-ion battery system based on a bipolar material $Na_2LiV_2(PO_4)_3$/C. *J. Mater. Chem. A* ***6***, 9962-9970.

6. Guo, S., Yu, H., Liu, P., Ren, Y., Zhang, T., Chen, M., Ishida, M., and Zhou, H. (2015). High-performance symmetric sodium-ion batteries using a new, bipolar O3-type material, $Na_{0.8}Ni_{0.4}Ti_{0.6}O_2$. *Energy Environ. Sci.* ***8***, 1237-1244.

7. Wang, Y., Xiao, R., Hu, Y.-S., Avdeev, M., and Chen, L. (2015). P2-$Na_{0.6}[Cr_{0.6}Ti_{0.4}]O_2$ cation-disordered electrode for high-rate symmetric rechargeable sodium-ion batteries. *Nat. Commun.* ***6***, 6954.

8. Wang, D., Bie, X., Fu, Q., Dixon, D., Bramnik, N., Hu, Y.-S., Fauth, F., Wei, Y., Ehrenberg, H., Chen, G.*, et al.* (2017). Sodium vanadium titanium phosphate electrode for symmetric sodium-ion batteries with high power and long lifespan. *Nat. Commun.* ***8***, 15888.

9. Wang, H., Chen, C., Qian, C., Liang, C., and Lin, Z. (2017). Symmetric sodium-ion batteries based on the phosphate material of NASICON-structured $Na_3Co_{0.5}Mn_{0.5}Ti(PO_4)_3$. *RSC Adv.* ***7***, 33273-33277.

10. Yao, Y., Zhang, L., Gao, Y., Chen, G., Wang, C., and Du, F. (2018). Assembly of $Na_3V_2(PO_4)_2F_3$@C nanoparticles in reduced graphene oxide enabling superior Na^+ storage for symmetric sodium batteries. *RSC Adv.* ***8***, 2958-2962.

11. Wang, Y., Zeng, J., Cui, X., Zhang, L., and Zheng, G. (2016). Separator-Integrated, Reversely Connectable Symmetric Lithium-Ion Battery. *Small* ***12***, 1091-1097.

12. Wang, S., Wang, L., Zhu, Z., Hu, Z., Zhao, Q., and Chen, J. (2014). All Organic Sodium-Ion Batteries with $Na_4C_8H_2O_6$. *Angew. Chem. Int. Ed.* ***53***, 5892-5896.

13. Zhao, Q., Wang, J., Lu, Y., Li, Y., Liang, G., and Chen, J. (2016). Oxocarbon Salts for Fast Rechargeable Batteries. *Angew. Chem. Int. Ed.* ***55***, 12528-12532.

14. Chi, X., Liang, Y., Hao, F., Zhang, Y., Whiteley, J., Dong, H., Hu, P., Lee, S., and Yao, Y. (2018). Tailored Organic Electrode Material Compatible with Sulfide Electrolyte for Stable All-Solid-State Sodium Batteries. *Angew. Chem. Int. Ed.* ***57***, 2630-2634.

15. Wang, S., Wang, L., Zhang, K., Zhu, Z., Tao, Z., and Chen, J. (2013). Organic $Li_4C_8H_2O_6$ Nanosheets for Lithium-Ion Batteries. *Nano Lett.* ***13***, 4404-4409.

16. Dai, G., He, Y., Niu, Z., He, P., Zhang, C., Zhao, Y., Zhang, X., and Zhou, H. (2019). A Dual-Ion Organic Symmetric Battery Constructed from Phenazine-Based Artificial Bipolar Molecules. *Angew. Chem. Int. Ed.* ***131***, 10007-10011.

17. Chen, H., Armand, M., Courty, M., Jiang, M., Grey, C.P., Dolhem, F., Tarascon, J.-M., and Poizot, P. (2009). Lithium Salt of Tetrahydroxybenzoquinone: Toward the Development of a Sustainable Li-Ion Battery. *J. Am. Chem. Soc.* ***131***, 8984-8988.